Redox Biology 69 (2024) 102992

Contents lists available at ScienceDirect

Redox Biology

journal homepage: www.elsevier.com/locate/redox

Superoxide dismutase 2 deficiency is associated with enhanced central chemoreception in mice: Implications for breathing regulation

Esteban Díaz-Jara [a], Katherine Pereyra [a], Sinay Vicencio [a], Margrethe A. Olesen [b], Karla G. Schwarz [a], Camilo Toledo [a,c], Hugo S. Díaz [a], Rodrigo A. Quintanilla [b], Rodrigo Del Rio [a,d,e,*]

[a] Laboratory of Cardiorespiratory Control, Pontificia Universidad Católica de Chile, Santiago, Chile
[b] Laboratory of Neurodegenerative Diseases, Universidad Autónoma de Chile, Santiago, Chile
[c] Institute of Physiology, Universidad Austral de Chile, Valdivia, Chile
[d] Centro de Excelencia en Biomedicina de Magallanes (CEBIMA), Universidad de Magallanes, Punta Arenas, Chile
[e] Department of Cell Biology and Physiology, School of Medicine, University of Kansas Medical Center, Kansas City, KS, United States

ARTICLE INFO

Keywords:
Superoxide
Ventilatory chemoreflex
Retrotrapezoid nucleus
SOD2
Central chemoreceptors

ABSTRACT

Aims: In mammals, central chemoreception plays a crucial role in the regulation of breathing function in both health and disease conditions. Recently, a correlation between high levels of superoxide anion ($O_2^{\cdot-}$) in the Retrotrapezoid nucleus (RTN), a main brain chemoreceptor area, and enhanced central chemoreception has been found in rodents. Interestingly, deficiency in superoxide dismutase 2 (SOD2) expression, a pivotal antioxidant enzyme, has been linked to the development/progression of several diseases. Despite, the contribution of SOD2 on $O_2^{\cdot-}$ regulation on central chemoreceptor function is unknown. Accordingly, we sought to determine the impact of partial deletion of SOD2 expression on i) $O_2^{\cdot-}$ accumulation in the RTN, ii) central ventilatory chemoreflex function, and iii) disordered-breathing. Finally, we study cellular localization of SOD2 in the RTN of healthy mice.

Methods: Central chemoreflex drive and breathing function were assessed in freely moving heterozygous SOD2 knockout mice ($SOD2^{+/-}$ mice) and age-matched control wild type (WT) mice by whole-body plethysmography. $O_2^{\cdot-}$ levels were determined in RTN brainstem sections and brain isolated mitochondria, while SOD2 protein expression and tissue localization were determined by immunoblot, RNAseq and immunofluorescent staining, respectively.

Results: Our results showed that $SOD2^{+/-}$ mice displayed reductions in SOD2 levels and high $O_2^{\cdot-}$ formation and mitochondrial dysfunction within the RTN compared to WT. Additionally, $SOD2^{+/-}$ mice displayed a heightened ventilatory response to hypercapnia and exhibited overt signs of altered breathing patterns. Both, RNAseq analysis and immunofluorescence co-localization studies showed that SOD2 expression was confined to RTN astrocytes but not to RTN chemoreceptor neurons. Finally, we found that $SOD2^{+/-}$ mice displayed alterations in RTN astrocyte morphology compared to RTN astrocytes from WT mice.

Innovation & conclusion: These findings provide first evidence of the role of SOD2 in the regulation of $O_2^{\cdot-}$ levels in the RTN and its potential contribution on the regulation of central chemoreflex function. Our results suggest that reductions in the expression of SOD2 in the brain may contribute to increase $O_2^{\cdot-}$ levels in the RTN being the outcome a chronic surge in central chemoreflex drive and the development/maintenance of altered breathing patterns. Overall, dysregulation of SOD2 and the resulting increase in $O_2^{\cdot-}$ levels in brainstem respiratory areas can disrupt normal respiratory control mechanisms and contribute to breathing dysfunction seen in certain disease conditions characterized by high oxidative stress.

* Corresponding author. Department of Cell Biology and Physiology University of Kansas Medical Center Kansas City, Kansas, United States.
E-mail addresses: efdiaz4@uc.cl (E. Díaz-Jara), kvpereyra@uc.cl (K. Pereyra), scvicencio@uc.cl (S. Vicencio), molesen.2@gmail.com (M.A. Olesen), karlaschwarz@uc.cl (K.G. Schwarz), camilo.toledo@uach.cl (C. Toledo), hdiaz@bio.puc.cl (H.S. Díaz), rodrigo.quintanilla@uautonoma.cl (R.A. Quintanilla), rdelrio@kumc.edu (R. Del Rio).

https://doi.org/10.1016/j.redox.2023.102992
Received 30 October 2023; Accepted 7 December 2023
Available online 12 December 2023

1. Introduction

Central chemoreception is essential for regulating breathing in mammals by sensing carbon dioxide (CO_2) and pH levels in the cerebrospinal fluid [20,22,32,39]. Enhanced central chemoreflex drive has been associated with irregular breathing and increased mortality in various disease conditions [11,24,30,31,36,41]. Indeed, potentiation of the ventilatory chemoreflex has been shown in heart failure, hypertension, chronic obstructive pulmonary disease, stroke, diabetes, sleep apnea and asthma. However, the precise molecular mechanisms underlying the potentiation of central chemoreflex drive remain incompletely understood.

Central chemoreceptors are primarily located on the ventral surface of the medulla, but they can also be found in other regions of the brainstem, hypothalamus, cerebellum, and midbrain, albeit in smaller numbers [15,20,32]. In rodents, the Retrotrapezoid nucleus (RTN) is a major brainstem region that regulates multiple aspects of breathing, such as inspiratory amplitude, breathing frequency, and active expiration in response to changes in brain CO_2 (PCO_2) levels [21,22,26,29,36]. Recent research has shown that removing some RTN chemoreceptor neurons using substance *P*-conjugated saporin toxin can normalize central chemoreflex and respiratory disorders in animals with heart disease, highlighting the significance of RTN neurons in the pathological process of central chemoreflex potentiation [11].

In addition to RTN chemoreceptor neurons, RTN astrocytes have gained attention for their role in regulating breathing through the release of various gliotransmitters that modulate RTN chemoreceptor neurons [19,37,40]. Studies from our laboratory have demonstrated that decreased expression of Glial fibrillary acidic protein (GFAP) in the RTN, indicative of reduced activity of RTN astrocytes, lead to RTN-mediated breathing disorders [40]. This suggests that RTN astrocytes contribute to the hyper-responsiveness of RTN chemoreceptor neurons. However, the precise molecular mechanisms underlying the dysfunction of RTN astrocyte-to-neuron communication remain elusive.

Superoxide radical ($O_2^{\cdot-}$) is known to play a pivotal role in the progression of several pathological conditions, including cardiovascular diseases [1,38,41,43]. Our recent study revealed a correlation between high levels of $O_2^{\cdot-}$ in the RTN and enhanced central chemoreflex drive in rats with chronic heart disease [12]. Interestingly, we found that reduced expression of superoxide dismutase 2 (SOD2) in the brainstem was associated with high chemoreflex sensitivity [12]. SOD2, encoded by the Sod2 gene, is a critical component of mitochondrial and cellular machinery involved in maintaining redox homeostasis and cellular protection during high $O_2^{\cdot-}$ levels [25]. However, no studies have investigated whether high $O_2^{\cdot-}$ or loss of SOD2 can regulate central chemoreflex function.

Therefore, in the present study, we aim to determine whether increased $O_2^{\cdot-}$ levels due to decreased SOD2 expression in the brainstem, particularly the RTN, lead to the potentiation of central chemoreflex drive and the development of disordered breathing in non-pathological conditions. This approach avoids confounding comorbidities present in animal disease models and supports a role of $O_2^{\cdot-}$ in central chemoreception.

Abbreviations

AHI	Apnoea–Hypopnoea Index
CV	Coefficient of Variation
DHE	Dihydroethidium
HCVR	Hypercapnic Ventilatory Response
HF	Heart failure
IS	Irregular Score
PeF	Peak Expiratory Flow
PiF	Peak Inspiratory Flow
RB	Resting Breathing
R_f	Respiratory frequency
ROS	Reactive Oxygen Species
RTN	Nucleus Retrotrapezoid
RVLM	Rostral Ventrolateral Medulla
SD1	Short Variability of Breath-to-Breath interval
SD2	Long Variability of Breath-to-Breath interval
SOD2	Superoxide Dismutase 2
T_e	Expiration time
T_i	Inspiration Time
T_{TOT}	Total Time
V_E	Ventilatory minute
V_T	Tidal Volume
V_T/T_I	Inspiratory Drive

2. Results

2.1. Oxidative stress markers are increased in brainstem from SOD2$^{+/-}$ mice

The heterozygous SOD2$^{+/-}$ mice employed in this study exhibit a notable reduction in SOD2 activity across multiple tissues [44]. Given that the decrease in SOD2 antioxidant protection results in elevated superoxide anion production, we employed various experimental approaches to assess oxidative stress in the brainstem of SOD2$^{+/-}$ and WT (wild-type) animals (Fig. 1A).

First, we determined $O_2^{\cdot-}$ levels in the brainstem using the $O_2^{\cdot-}$ sensitive fluorescent dye dihydroethidium (DHE) in fresh slices. SOD2$^{+/-}$ mice showed a ~3.0-fold increase in DHE staining in the RTN compared with WT animals (DHE $_{RTN}$: 1.00 ± 0.21 vs. 3.22 ± 0.85 A U. WT vs SOD2$^{+/-}$; $p < 0.05$) (Fig. 1B). Later, we evaluated two oxidative stress markers by immunofluorescence in brainstem fixed slices: nitrotyrosines, a product of tyrosine nitration mediated by reactive nitrogen species such as peroxynitrite anions and nitrogen dioxide (n-Tyr; Fig. 1C), and 8-hydroxyguanosine, a common DNA damage marker resulting from elevated reactive oxygen species (8-OHdG; Fig. 1D). n-Tyr staining showed a ~2.5-fold increase in the RTN region in SOD2$^{+/-}$ animals compared with WT group (n-Tyr $_{RTN}$: 1.00 ± 0.03 vs. 2.47 ± 0.10 A U. WT vs SOD2$^{+/-}$; $p < 0.05$) (Fig. 1C). In addition, SOD2$^{+/-}$ animals displayed a ~2.5-fold increase of 8-OHdG staining in the RTN region compared to WT animals (8-OHdG $_{RTN}$: 1.00 ± 0.08 vs. 2.41 ± 0.12 A U. WT vs SOD2$^{+/-}$; $p < 0.05$) (Fig. 1D). Also, we found that SOD2$^{+/-}$ mice displayed a ~30 % reduction in SOD2 expression compared to WT mice at the level of RTN (Fig. 1E). Lastly, we decided to performed experiments in brain isolated mitochondria to evaluate mitochondrial ROS considering SOD2 primarily sub-cellular location (Fig. 1A). We found a trend for reduced ATP production in mitochondria obtained from SOD2$^{+/-}$ compared to WT that did not reach statistical significance (Fig. 1F). But, SOD2$^{+/-}$ mice exhibit a significant reduction in brain mitochondrial membrane potential ($_{\psi}$Potential: 1.00 ± 0.02 vs. 0.84 ± 0.03 A U; WT vs SOD2$^{+/-}$; $p < 0.05$) along with marked increases in superoxide production (Mitosox: 1.00 ± 0.08 vs. 1.29 ± 0.05 A U; WT vs SOD2$^{+/-}$; $p < 0.05$) compared to WT mice (Fig. 1G).

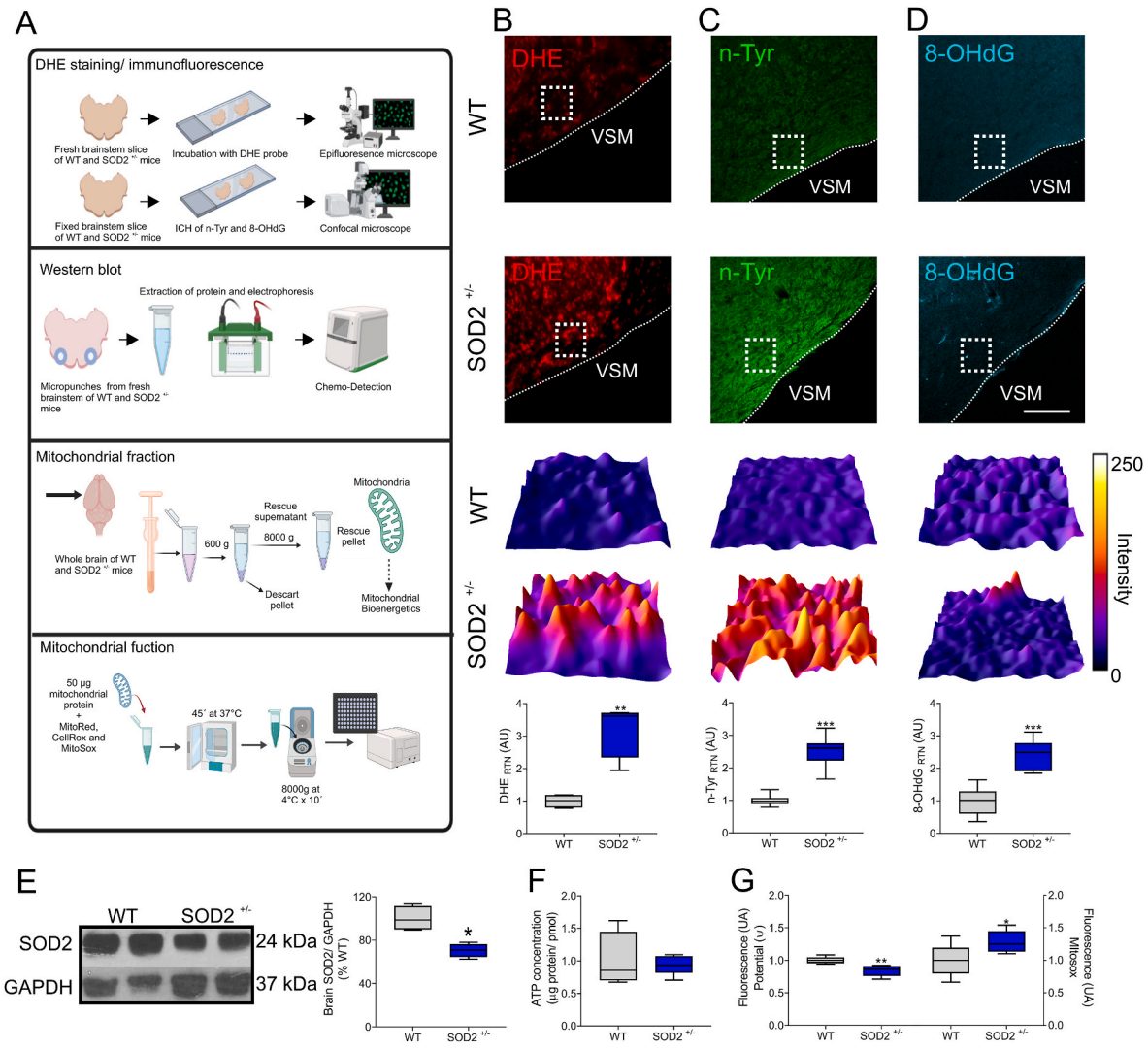

Fig. 1. Determination of superoxide levels, oxidative stress markers and mitochondrial function in WT and SOD2$^{+/-}$ mouse brains. (A) Flowchart representation detailing the stepwise methodologies employed, from tissue extraction to mitochondrial functional assays: DHE staining, immunofluorescence, Western blot, and mitochondrial fractions. (B) Representative brainstem slices stained with dihydroethidium (DHE) to detect superoxide in wild type (WT) and SOD2$^{+/-}$ mice (total magnification: 40×). RTN 3D surface colormap of fluorescent intensity from DHE staining showed in (A) and the summary data of DHE RTN fluorescent intensity normalized by the intensity obtained in the WT group. (C–D) Representative brainstem slices stained with nitro-tyrosine (n-Tyr) and 8-hydroxyguanosine (8-OHdG), respectively, to detect oxidative stress biomarkers in the RTN of WT and SOD2$^{+/-}$ mice (total magnification: 40×). RTN 3D surface colormap of fluorescent intensity from n-Tyr and 8-OHdG staining showed in (C and D) and the summary data of n-Tyr RTN and 8-OHdG RTN fluorescent intensity normalized by the intensity obtained in the WT group. (E) Representative immunoblots of SOD2 expression in RTN micropunches. Summary data showing SOD2 expression. (F) ATP content in the brain tissue from WT mice and SOD2$^{+/-}$ mice (G) Mitochondrial membrane potential and superoxide mitochondrial production measured by quantitative analysis of fluorescence intensity of TMRE and MitoSox Red in an isolated mitochondrial fraction. Boxplots showing max and min *p < 0.05; **p < 0.01; ***p < 0.001. vs. WT, Student's *t*-test (unpaired). WT, n = 4, SOD2$^{+/-}$; n = 4. (For interpretation of the references to color in this figure legend, the reader is referred to the Web version of this article.)

2.2. SOD2 deficiency contributes to enhance central chemoreflex function and induces disordered breathing

We found that SOD2$^{+/-}$ mice showed a significant elevation in resting minute ventilation compared to WT mice (Supplementary Table 1). Indeed, minute ventilation was ~2-fold higher in SOD2$^{+/-}$ mice compared to WT animals (V_E: 2.59 ± 0.19 vs. 4.48 ± 0.70 mL/min 10 g. WT vs SOD2$^{+/-}$; $p < 0.05$) (Supplementary Table 1). Considering the elevated levels of superoxide in the RTN in SOD2$^{+/-}$ mice, we assessed the ventilatory response to hypercapnia by unrestrained whole-body plethysmography (Fig. 2A). We found that SOD2$^{+/-}$ mice exhibited an heightened ventilatory response to hypercapnia compared to WT mice (Fig. 2B). Additionally, SOD2$^{+/-}$ mice displayed an increased central chemoreflex sensitivity compared to WT group (ΔV_E: 1.84 ± 0.36 vs. 3.87 ± 0.16 mL/min/10 g; HCVR: 0.26 ± 0.05 vs. 0.55 ± 0.02 ΔV_E^{-1} WT vs SOD2$^{+/-}$; $p < 0.001$) (Fig. 2C and D). Furthermore, SOD2$^{+/-}$ mice displayed higher tidal volume (V_T), V_E and peak inspiratory flows (PiF) than the WT animals under both normoxic and hypercapnic conditions (Supplementary Table 1).

Next, we evaluated whether deficiency in SOD2 expression triggers disordered breathing. Our results showed that SOD2$^{+/-}$ mice displayed irregular breathing patterns at rest (Fig. 3A). Compared to WT group, SOD2$^{+/-}$ animals exhibited greater breath-to-breath interval variability (Fig. 3B) and non-symmetrical distribution of ventilatory cycles (Fig. 3C). Indeed, SOD2$^{+/-}$ mice showed an increased short (SD1) and long-term (SD2) variability of the breath-to-breath interval compared to WT mice (SD1: 26.80 ± 6.49 vs. 43.58 ± 17.22 ms; SD2: 28.90 ± 6.20 vs. 61.40 ± 17.35 ms; WT vs SOD2$^{+/-}$; $p < 0.05$) (Fig. 3D and E).

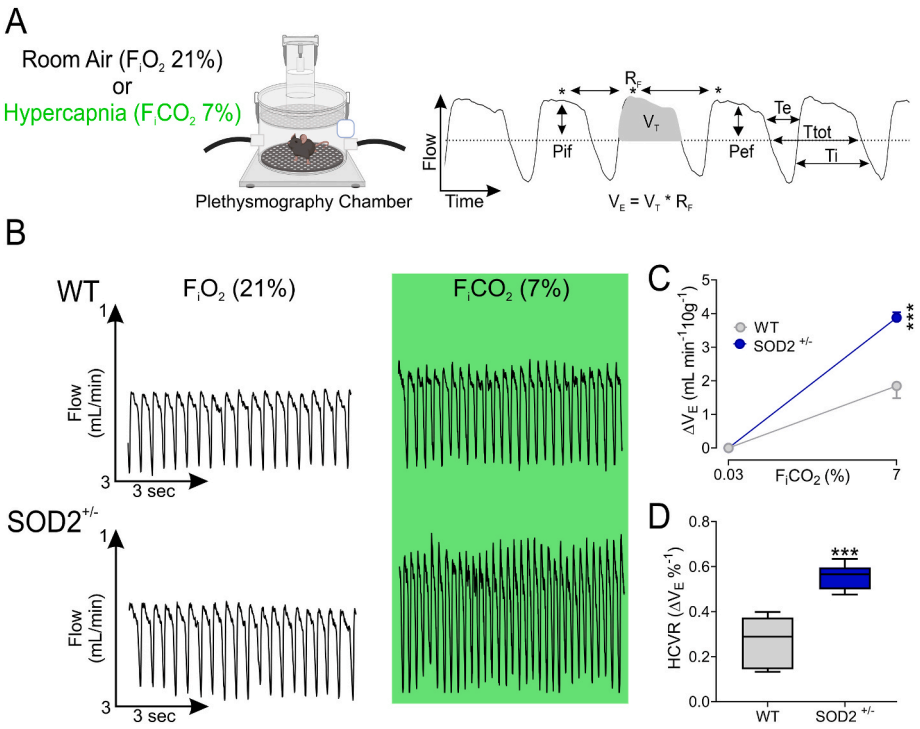

Fig. 2. Central chemoreflex drive is exacerbated in SOD2$^{+/-}$ mice. (A) Schematic of experimental setup and example of plethysmograph recording showing all quantified ventilatory parameters. (B) Representative recordings of ventilatory flow during chemoreflex test in normoxia (F_iO_2 21 %) and during hypercapnia (F_iCO_2 7 %) in one WT mice and one SOD2$^{+/-}$ mice. **(C)** Summary data showing changes in V_E during hypercapnic stimulus in WT mice and SOD2$^{+/-}$ mice. **(E)** Summary data showing changes in the gain of the hypercapnic ventilatory response (HCVR) in all groups. Boxplots showing max and min. ***,$p < 0.001$ vs. WT, Student's *t*-test (unpaired). WT, n = 5, SOD2$^{+/-}$, n = 6.

Furthermore, SOD2$^{+/-}$ mice presented higher V_T variability compared to WT animals (CV: 11.30 ± 2.35 vs. 23.48 ± 3.57 % WT vs SOD2$^{+/-}$; $p < 0.001$; Fig. 3F). Moreover, we found that SOD2$^{+/-}$ mice displayed higher irregularity score (IS) compared with WT animals (5.15 ± 1.51 vs. 8.43 ± 1.12 %, WT vs SOD2$^{+/-}$; $p < 0.001$; Fig. 3G). This was paralleled by significant increases in the incidence of apneas/hypopneas in SOD2$^{+/-}$ mice (Supplementary Table 2). Specifically, the incidence of apneas/hypopneas (AHI) in SOD2$^{+/-}$ mice was twice as high as in WT mice (AHI: 4.33 ± 2.33 vs. 8.00 ± 3.16 events/h; %, WT vs SOD2$^{+/-}$; $p < 0.05$.) (Supplementary Table 2). No differences were observed between groups in terms of apnea and post-sigh apnea duration, neither in the number of sigh and post-sigh apneas (Supplementary Table 2). Lastly, we identified a positive correlation between DHE $_{RTN}$ levels in the RTN and central chemoreflex drive and irregular breathing specifically in SOD2$^{+/-}$ mice (Fig. 3H; Supplemental Figure 1). However, no correlation within these variables were found in WT mice (Fig. 3H; Supplemental Figure 1).

2.3. *Specific SOD2 cell-type localization and expression within the mice RTN*

We evaluated the subcellular localization of SOD2 in fixed brain sections containing the RTN. To achieve this, we employed specific antibodies against SOD2, Paired-like homeobox 2b (Phox2b, marker of the RTN chemoreceptor neuron), Glial fibrillary acidic protein (GFAP, astrocyte marker). Co-localization analysis of Phox2b, and SOD2 with GFAP is shown in Fig. 4. No co-localization was found between SOD2 and Phox2b positive neurons throughout the brainstem region (Fig. 4A). Conversely, analysis of 3D reconstructions and orthogonal views revealed that SOD2 co-localized with GFAP staining (Fig. 4B). In addition to SOD2 immunolocalization studies within the RTN, we performed single-cell RNAseq data validation. We identified 1,516 SOD2-positive cells (expressing Sod2 gene) from the mouse ventral parafacial medulla (Fig. 4C). Then, we selected clusters with known cell-type specific marker genes relevant for RTN physiology (i.e. chemoreceptor neurons, astrocytes) (Fig. 4D and E).

RTN chemoreceptor neuron cluster was defined as cells expressing Syn1 (Synapsin-1), Slc17A6 (Vglut2), Slc32a1 (Vgat), Phox2b, Gal (Galanin), Nmb (Neuromedin-B), Grp4 (G Protein-Coupled Receptor 4, a pH-sensitive receptor), Kcnk5 (Task-2, the other pH-sensitive receptor of RTN chemoreceptors neurons) and Tacr1 (Tachykinin Receptor 1). On the other hand, RTN astrocytes cluster was defined as cells expressing GFAP, Aldoc (Aldose), Aqp4 (Aquaporin-4) and Slc4a4 (sodium bicarbonate cotransporter) (Fig. 4D). After categorizing the clusters (Fig. 4D), we determined the expression of Sod2 gene expression between the clusters. Our analysis revealed significantly higher Sod2 gene expression in the cluster associated with RTN astrocytes compared to the RTN neuron cluster (Fig. 4F). Finally, compared to other genes related to antioxidant activity (i.e. catalase, glutathione peroxidase) expressed by RTN astrocytes, we found that Sod2 gene is significantly more abundant in the RTN of mice under physiological conditions (Supplemental Figure 2).

2.4. *SOD2$^{+/-}$ mice displayed altered astrocyte morphology and density in the RTN*

To assess the impact of partial SOD2 expression in RTN astrocytes we studied RTN astrocyte morphology and density through Sholl analyses of GFAP-immunolabeled cells within the RTN of WT and SOD2$^{+/-}$ animals. Representative confocal images of GFAP-labeled astrocytes are depicted in Fig. 5A and B. Compared to WT group, SOD2$^{+/-}$ astrocytes showed a reduction in both total length and the number of branches (Total length: 248.2 ± 9.98 vs. 211.9 ± 9.75 μm; # of branches: 19.7 ± 0.99 vs. 16.6 ± 0.75, WT vs SOD2$^{+/-}$; $p < 0.05$; Fig. 5C and D). Indeed, the convex hull volume of RTN astrocytes in SOD2$^{+/-}$ mice, which is an indicator of cell complexity, was markedly lower compared to RTN

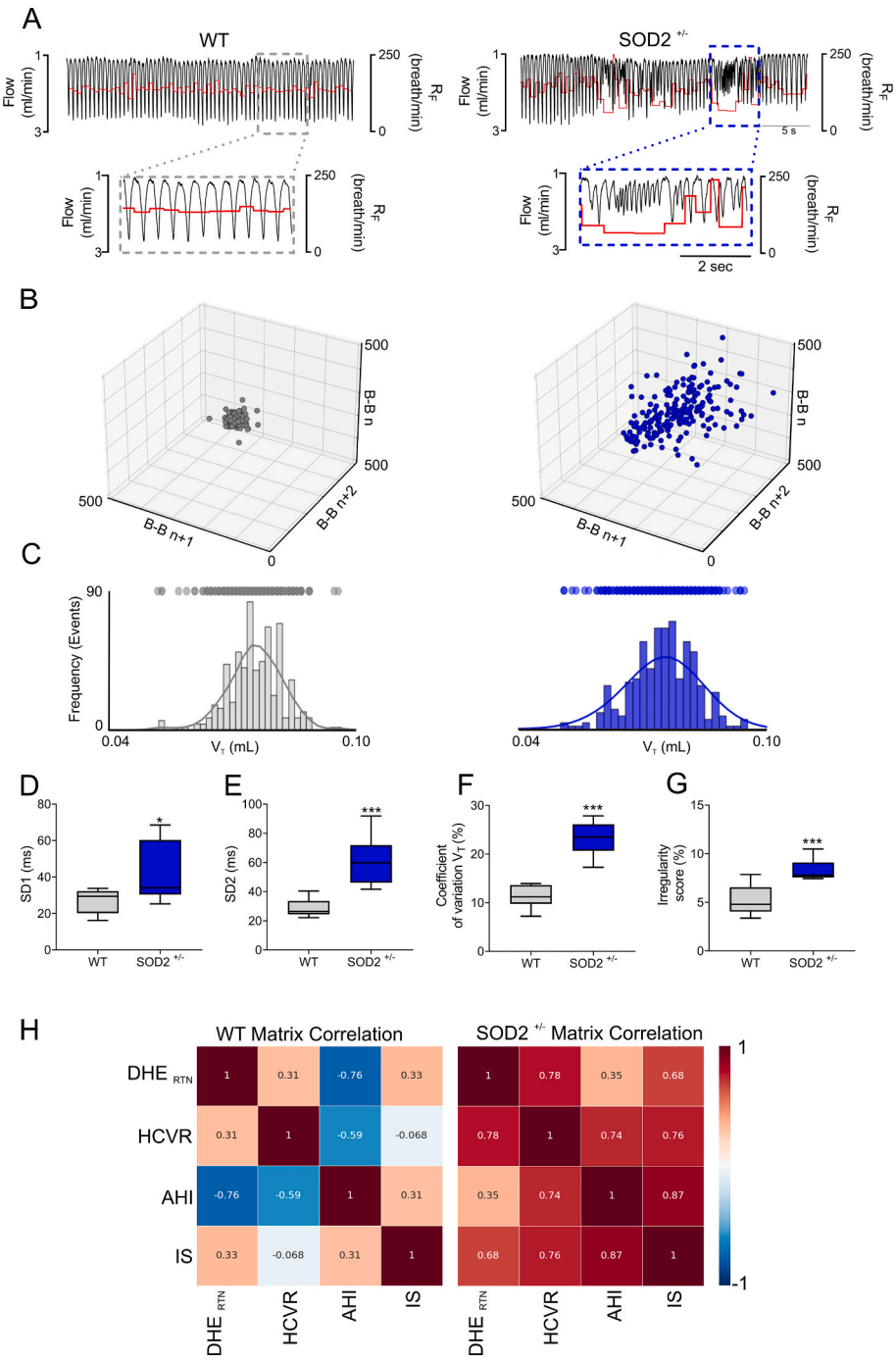

Fig. 3. SOD2$^{+/-}$ mice display disordered-breathing. Resting breathing patterns and breathing disorders were evaluated in freely moving mice. (A) Representative traces of resting ventilatory flow and respiratory frequency from one WT and one SOD2$^{+/-}$ mice. Note that SOD2$^{+/-}$mice displays irregular breathing pattern with unstable respiratory frequency. (B) Representative 3D Poincare plot showing breath-to-breath (B–B) interval variability in one WT and one SOD2$^{+/-}$ mice. (C) Representative frequency histogram showing the distribution of tidal volume (V_T) amplitude diversity in one WT and one SOD2$^{+/-}$ mice. (D,E) Summary data showing short (SD1) and long term (SD2) B–B interval variability, respectively. (F) Summary data showing coefficient of variation of V_T. (G) Summary data showing breathing irregularity score in both groups. (H) Correlation matrix of ventilatory variables, breathing irregularity variables and brainstem ROS levels. Boxplots showing max and min. *, $p < 0.05$; ***, $p < 0.001$ vs. WT, Student's *t*-test (unpaired). WT, n = 5, SOD2$^{+/-}$, n = 6.

astrocytes from WT mice (Convex Hull Boundary Size: 2,382 ± 125.7 vs. 2,002 ± 122.3 μm^2, WT vs SOD2$^{+/-}$; $p < 0.05$; Fig. 5E). However, we did not observe any changes in the number of intersections along radial distance from the soma nor in the maximum intersection radius or branches length between WT and SOD2$^{+/-}$ mice (Supplemental Figure 3). Finally, we found that SOD2$^{+/-}$ mice exhibited a ~50 % decrease in GFAP staining intensity in the RTN compared to WT mice (Supplemental Figure 3).

3. Discussion

The main aim of our study was to determine if reductions in SOD2, a key antioxidant enzyme, lead to redox imbalance in chemosensory regions involved in central chemoreflex regulation. The major findings of our study are as follows: i) SOD2$^{+/-}$ mice exhibited oxidative stress in the brainstem, with elevated ROS levels detected specifically in the RTN region, ii) ROS accumulation in the RTN was associated with heightened

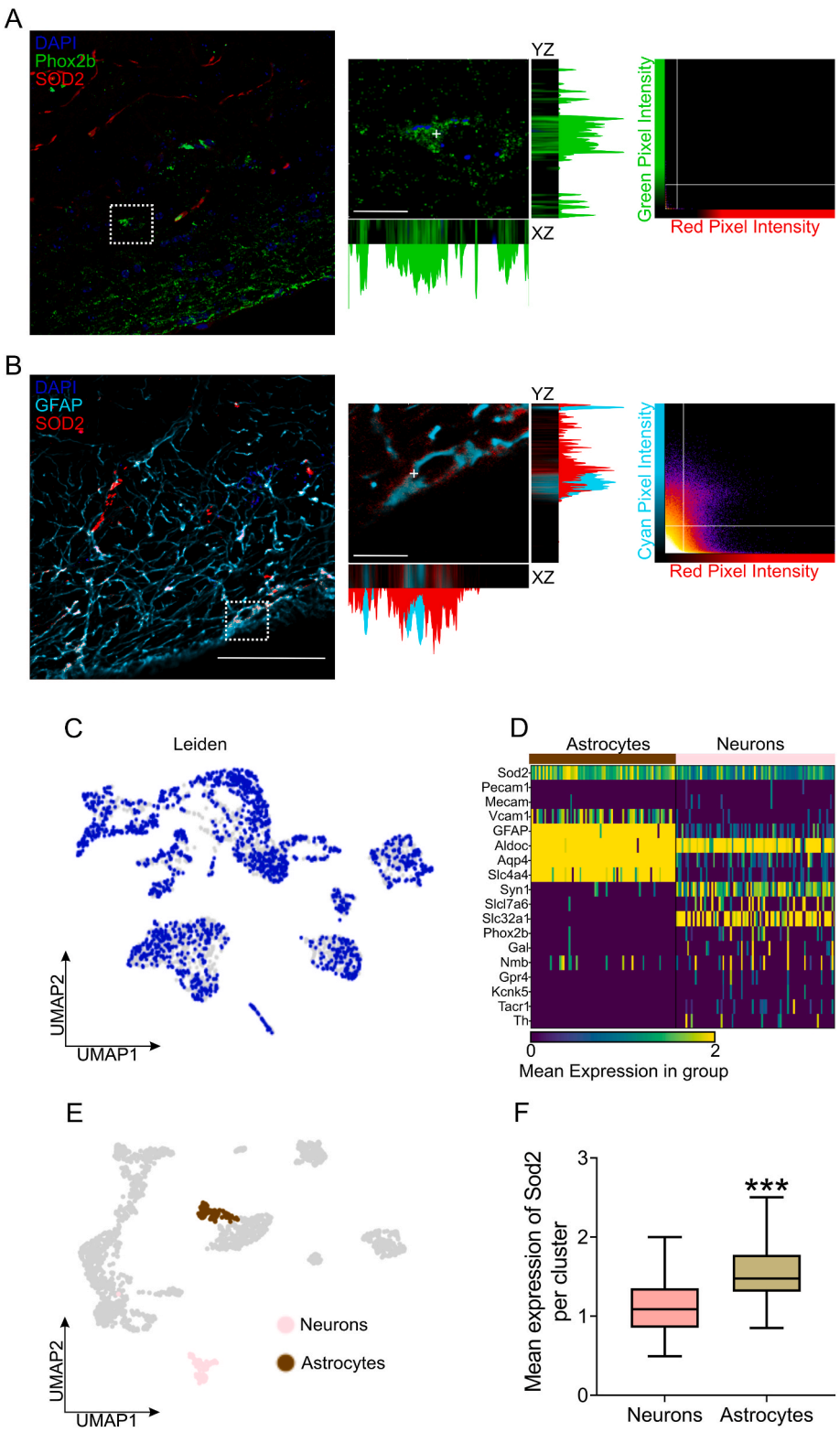

Fig. 4. SOD2 localization within the RTN of mice. (A,B) Representative fluorescent images depicting staining for SOD2 (red), Phox2b (green) and GFAP (green) in RTN slices obtained in one WT animal. Scalebar: 50 μm. Insets indicate orthogonal views and intensity plots of the co-localization of SOD2 with Phox2b (A) and GFAP (B) staining. Scalebar: 10 μm. (C) Visualization of positive cells for Sod2 gene in ventral parafacial single-cell mRNA sequencing data. (D) Heatmap of the expression of Sod2, astrocytes gene markers (GFAP, Aldoc (Aldose), Aqp4 (Aquaporin-4) and Slc4a4 (sodium bicarbonate cotransporter)) and RTN neurons gene markers (Syn1 (Synapsin-1), Slc17A6 (Vglut2), Slc32a1 (Vgat), Phox2b, Gal (Galanin), Nmb (Neuromedin-B), Grp4 (G Protein-Coupled Receptor 4, a pH-sensitive receptor), Kcnk5 (Task-2, the other pH-sensitive receptor of RTN chemoreceptors neurons), Tacr1 (Tachykinin Receptor 1). (E) Isolation of RTN clusters containing neurons and astrocytes. (F) Summary data showing the mean expression of Sod2 gene in RTN chemoreceptors neurons and RTN astrocytes. Boxplots showing max and min. ***, $p < 0.001$ vs. RTN chemoreceptor neurons, Student's *t*-test (unpaired). RTN neurons, n = 86 cells; RTN astrocytes, n = 78 cells. (For interpretation of the references to color in this figure legend, the reader is referred to the Web version of this article.)

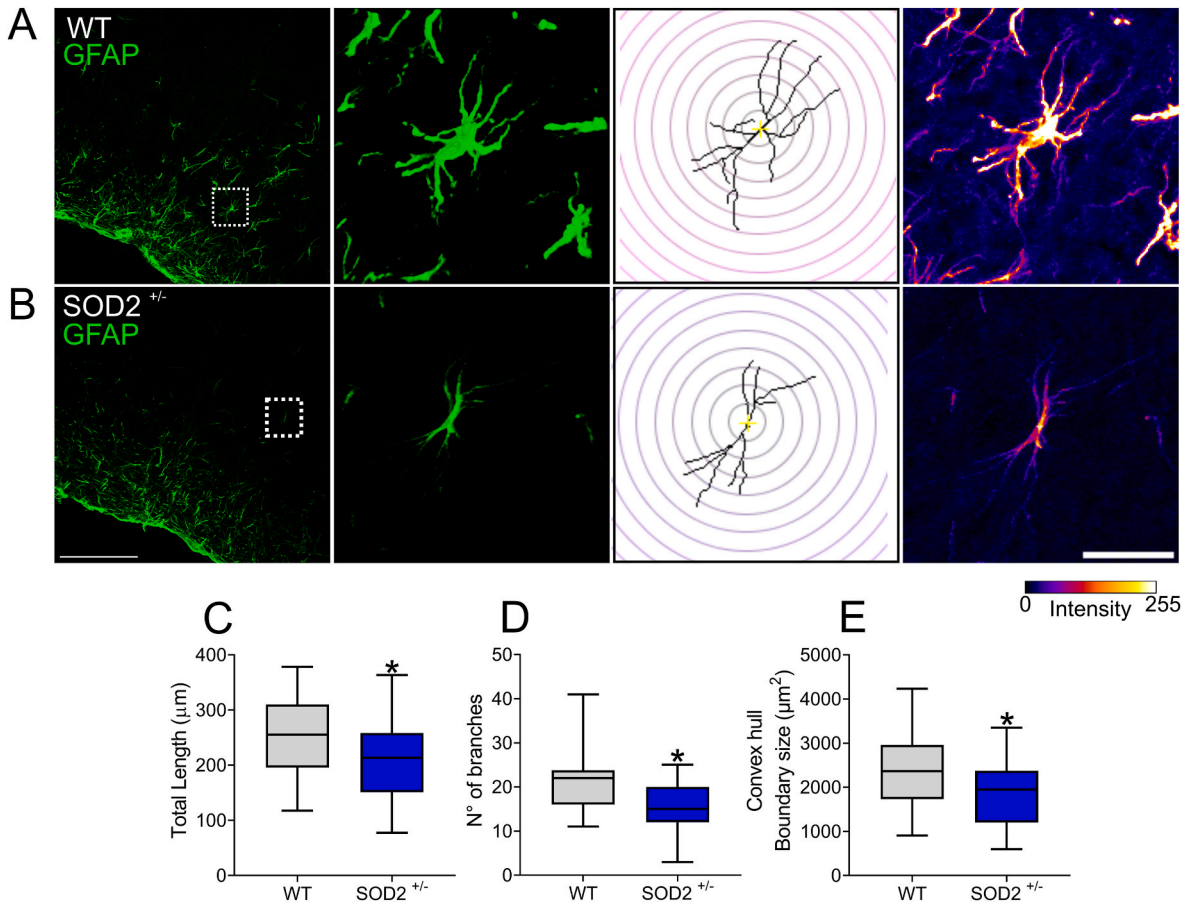

Fig. 5. Morphological changes in RTN astrocytes from SOD2$^{+/-}$ mice. (A,B) Representative RTN astrocytes immuno-stained with GFAP (green) in one WT mice (A) and one SOD2$^{+/-}$ mice (B) (magnification: 40×, scale bar: 100 µm). White dotted line box indicates examples of astrocytes selected for Sholl analysis. Scale bar: 20 µm. Heatmap color scale display GFAP fluorescence intensity. (C) Summary data showing astrocyte processes total length. (D) Summary of number of branches. (E) Summary of the complexity (Convex hull boundary size). Boxplots showing max and min. *, $p < 0.05$; ***,$p < 0.001$ vs. WT, Student's *t*-test (unpaired). WT, n = 4, SOD2 $^{+/-}$, n = 4. (For interpretation of the references to color in this figure legend, the reader is referred to the Web version of this article.)

central chemoreflex drive and the development of disordered breathing, iii) Within the RTN, SOD2 expression was found to co-localize with astrocyte and endothelial cell markers, but not with RTN chemoreceptor neurons, and iv) RTN astrocytes from SOD2$^{+/-}$ mice exhibited notable morphological alterations. Our results suggest that reduced expression of SOD2 in the RTN leads to the formation of ROS, which contributes, at least in part, to an increase in central chemoreceptor sensitivity, ultimately resulting in the development of breathing disorders (Fig. 6).

3.1. Loss of SOD2 and brainstem ROS levels

ROS levels, including superoxide and hydrogen peroxide, in the brainstem have been implicated in the pathogenesis and progression of various diseases [1,38]. Selective elimination of SOD2 in the subfornical organ (SFO) has been reported to increase mitochondrial superoxide production in the brain, playing a significant role in the development of angiotensin II-mediated hypertension [6]. Our recent findings demonstrated increased ROS levels in the RTN of rats with chronic heart disease, which were correlated with changes in breathing patterns [12]. While existing evidence supports the involvement of ROS in cardiorespiratory regulation, the specific contribution of SOD2-mediated ROS regulation on chemoreflex function remains unknown. The heterozygous SOD2$^{+/-}$ mice employed in this study exhibit a notable reduction in SOD2 activity across multiple tissues. Indeed, SOD2 activity in the brains of 4-month-old SOD2$^{+/-}$ animals decreases by almost 80 % compared to their WT (wild-type) counterparts [44]. Interestingly, it has been described that the SOD2 $^{+/-}$ mice does not display changes in the activity nor expression of other antioxidant enzymes such as SOD1, catalase, and glutathione peroxidase in the brain. However, these animals demonstrate an adaptive response to increased oxidative stress, as evidenced by the reduction in both oxidized (GSSG) and reduced (GSH) glutathione forms in the brain. These results align with the findings of Fulton et al., in 2021, where a complete SOD2 deletion mice model (SOD2$^{-/-}$) showed an upregulation of the Nrf 2 pathway as an adaptive response to glutathione production [16]. In this study, we provide the first evidence that partial deficiency in SOD2 expression leads to ROS accumulation in the brainstem, particularly in areas involved in respiratory regulation. Therefore, our present results further support and confirm previous findings indicating that brainstem regions are vulnerable to oxidative stress-induced damage resulting from altered SOD2 expression.

3.2. SOD2-mediated ROS regulation and central chemoreflex drive

Central chemoreceptors play a critical role in regulating breathing and maintaining pH balance but heightened central chemosensitivity has been associated with the development of abnormal breathing patterns [24]. Various mechanisms have been proposed to contribute to the potentiation of central chemoreflex in pathological conditions. However, the impact of SOD2, a crucial component of the cells antioxidant defense system, on central chemosensitivity remains unexplored. But, there is existing evidence indicating that reactive oxygen species (ROS) play a crucial role in the modulation of certain ion channels, such as K2P channels [10,35]. For instance, previous studies have shown that ROS

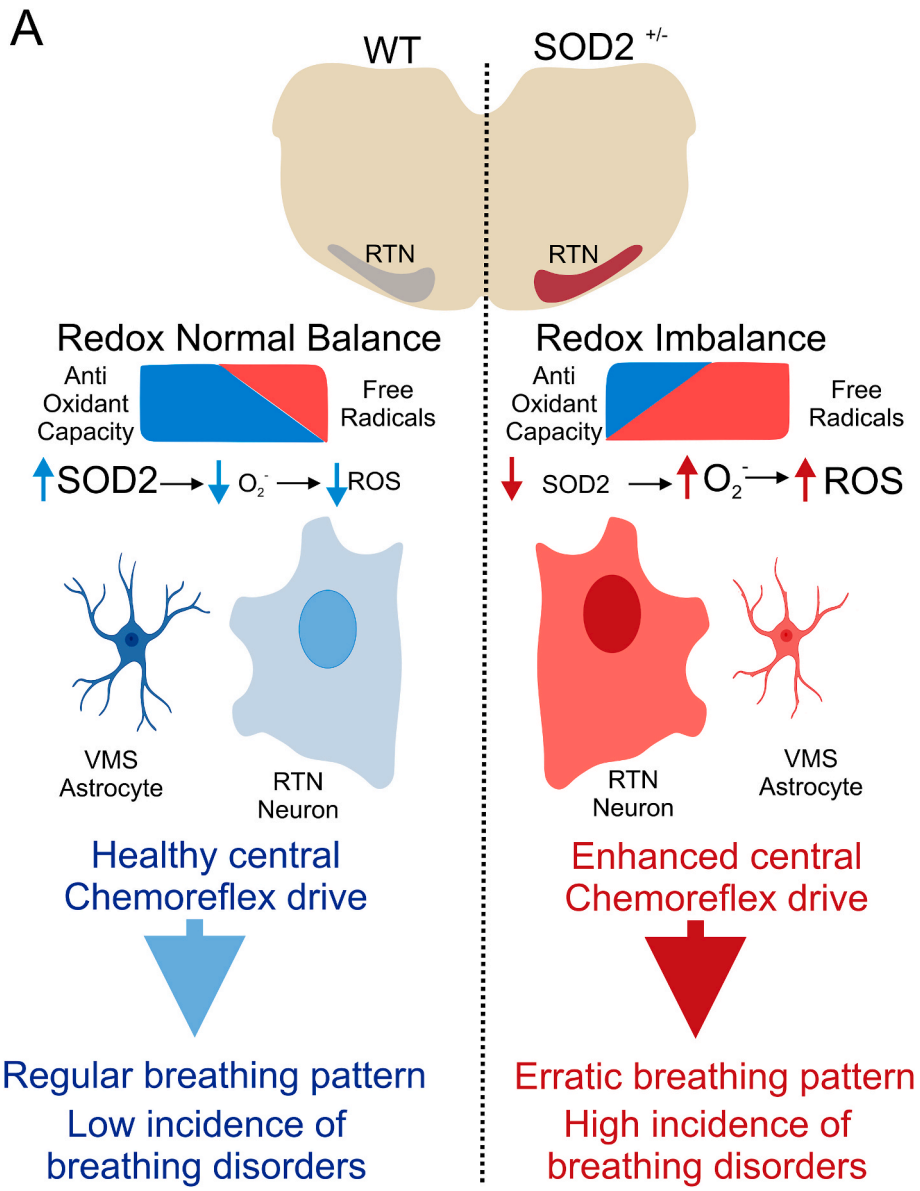

Fig. 6. SOD2 partial deficiency results in ROS accumulation within the RTN and potentiates central chemoreflex drive. In a healthy state, maintaining a balanced redox environment is crucial for keeping intracellular ROS levels low within RTN neurons. This balance is closely linked to normal central chemoreflex function and the preservation of regular resting breathing patterns. However, in SOD2$^{+/-}$ mice, the reduction of SOD2 expression levels disrupts this redox equilibrium, resulting in an increase in oxidative status. This shift leads to heightened central chemoreflex sensitivity, the emergence of irregular breathing patterns, and morphological changes in astrocytes, characterized by shorter length, fewer branches, and simplified morphology. Importantly, this mechanism may underlie the development of augmented RTN-mediated central chemoreflex drive and the subsequent occurrence of breathing disorders observed in experimental heart failure.

can inhibit TASK-3 channels in peripheral chemoreceptor cells, likely through the oxidation of cysteine residues in the TASK-3 protein [16]. Additionally, other channels like TREK2 and TASK-2 have also been reported to be modulated by intracellular oxidizing agents [17], leading to changes in cell excitability [10,33]. Considering this background, we can propose a plausible hypothesis that increased ROS production within the RTN might alter TASK-2 channel biophysical properties, potentially leading to higher H^+-mediated inhibition resulting in enhanced chemoreceptor neuron activity. This interesting hypothesis requires to be thoroughly tested in future experiments [34].

In this study, we investigated the effects of SOD2 partial down-regulation in animals without pre-existing pathology and demonstrated, for the first time, that the accumulation of ROS within the brainstem leads to an augmented ventilatory response to hypercapnia. This suggests that the loss of SOD2 in the RTN may contribute to the enhancement of central chemoreflex drive. Further research is required to fully validate this hypothesis.

3.3. *Partial SOD2 deficiency increases the incidence of breathing disorders*

Augmented central chemoreflex drive has been associated with the development of breathing disorders and irregular breathing patterns [3]. We recently demonstrated that the activation of RTN chemoreceptor neurons induces breathing disorders in healthy animals [40]. However, the impact of elevated ROS levels in the RTN on the occurrence of breathing disorders in healthy animals has not been previously investigated. In this study, we observed that SOD2$^{+/-}$ mice exhibited irregular breathing patterns at rest compared to WT mice. Importantly, we identified a positive correlation between ROS levels in the RTN and the manifestation of breathing alterations. These findings align with our previous research, which demonstrated that exercise training, known for

its ability to reduce oxidative stress, improves respiratory function in rats with heart disease [12]. Thus, our results strongly support the hypothesis that ROS accumulation in the RTN enhances chemoreceptor neuron sensitivity, augments central chemoreflex, and contributes to the development of breathing disorders [8].

3.4. SOD2 expression pattern in the RTN

Superoxide dismutase 2 (SOD2) is expressed ubiquitously throughout the body, including the brain, where it plays a critical role in protecting cells from oxidative stress [13]. It is also present in astrocytes and endothelial cells, which are essential for proper brain function [4,14]. In astrocytes, SOD2 functions as a key enzyme in maintaining redox balance by scavenging ROS and safeguarding against oxidative damage [2]. Similarly, SOD2 in endothelial cells is vital for maintaining low ROS levels, which is necessary for preserving the integrity of the blood-brain barrier (BBB) [23]. Elevated ROS levels can lead to BBB disruption, vasoconstriction, dysfunction of the neurovascular unit, and a decrease in nitric oxide levels, an important signaling molecule for vascular dilation [5,18,27].

Understanding the specific cellular localization of SOD2 within the mammalian RTN is crucial for elucidating its potential role in chemoreflex regulation. Additionally, we observed marked changes in astrocyte morphology upon partial SOD2 expression. RTN astrocytes from $SOD2^{+/-}$ mice displayed a loss of cellular complexity, indicating inhibition likely mediated by ROS production within the RTN. Interestingly, prior studies have reported that partial deletion of the SOD2 gene in hippocampal astrocytes leads to a decrease morphology of these cells, impacting cognitive function [2]. Additionally, Sobhrino et al. showed that chemical-induced inhibition of RTN astrocytes increases the firing frequency of chemoreceptor neurons in the RTN [37]. Together, these evidences suggests that inhibition of astrocytes impacted neuronal cell function towards a more excitable state. Therefore, it is plausible to hypothesize that the partial loss of SOD2 and the subsequent increase in superoxide production may contribute, at least in part, to inhibit RTN astrocytes being the outcome an impaired neuron-to-glia communication within the RTN that finally impact on central chemoreception. Future experiments should be directed towards addressing this novel hypothesis.

Other alternative hypothesis suggests that alterations in SOD2 expression within RTN blood vessels can affect blood perfusion to the region, leading to metabolic inhibition of astrocytes in the RTN. Previous studies have demonstrated that ROS-induced constriction of brain vessels and reduced blood flow to the RTN can enhance chemoreceptor activity and respiratory output in rodents [9].

Therefore, it is plausible to hypothesize that decreased SOD2 levels may impact blood perfusion to the RTN, resulting in changes in astrocyte physiology and disrupting glia-to-neuron communication, ultimately potentiating central chemoreflex drive. Further research is needed to investigate the molecular mechanisms underlying the effects of reduced SOD2 expression in astrocytes and endothelial cells on the physiology of RTN chemoreceptor neurons.

3.5. Study limitations

In the present study, we utilized heterozygous $SOD2^{+/-}$ mice as an experimental model to investigate the impact of partial SOD2 deletion on central chemoreception. However, there are certain limitations that should be acknowledged. Firstly, it is important to note that the partial deletion of SOD2 expression in this model is systemic and not restricted solely to the RTN level. Secondly, caution is required when extrapolating our findings from this model to more complex pathological conditions since our model does not fully replicate the intricacies of disease settings. Thirdly, although we observed changes in breathing patterns and heightened central chemoreflex drive in $SOD2^{+/-}$ mice, it remains unclear whether these alterations are solely attributed to the reduction of SOD2 expression in the RTN or if they are influenced by other chemoreceptor regions within the brain. Another limitation of our study is that both DHE and Mitosox reagents used to assess superoxide production, do not offer complete specificity in detecting superoxide anion exclusively [7]. While Mitosox provides a more targeted evaluation within mitochondria, potential interactions with other reactive oxygen species cannot be completely ruled out. Therefore, future studies with more advanced and specific superoxide detection methods may be needed to improve our understanding of the redox dynamics in the RTN. Therefore, upcoming studies should aim to provide evidence regarding the role of SOD2 in other central chemoreflex areas throughout the brain. Lastly, while we have identified RTN astrocytes as a primary cellular source of SOD2 expression, further investigations are necessary to precisely determine the involvement of astrocytic SOD2 in RTN chemoreception.

4. Innovation

The present study demonstrates that decreased SOD2 expression results in elevated ROS levels in the RTN, enhanced central chemoreflex drive, and breathing irregularities in mice. Additionally, we have identified, for the first time, higher constitutive expression of SOD2 in RTN astrocytes compared to other cell types. These findings provide valuable insights into the regulatory role of SOD2 in central chemoreflex function and lay the groundwork for future research aimed at developing innovative approaches targeting SOD2 for the treatment of breathing disorders associated with heightened central chemoreflex drive.

5. Materials and methods

5.1. Ethical approval and animals

Experiments were performed in male Heterozygous Sod2tm1Leb/J mice ($SOD2^{+/-}$; breeding pairs), congenic in the C57BL/6J background, and C57BL/6J mice (2–4 months), were originally obtained from The Jackson Laboratory (Sacramento, CA, USA). Animals were facilitated by Dr. Waldo Cerpa from Pontificia Universidad Católica de Chile. The animals were housed at controlled room temperature under a 12 h light/dark cycle with *ad libitum* access to food and water. Experimental protocols were approved by the Bioethical Committee for Animal Experiments of the Pontificia Universidad Católica de Chile (protocol ID 210427016) in accordance with the standard of the National Institutes of Health (NIH) and the Guide for the Care and Use of Laboratory Animals. At the end of the experiments, all animals were euthanized via overdose of sodium pentobarbital (100 mg/kg i.p.).

5.2. Resting breathing and ventilatory chemoreflex function

Resting breathing (RB) and chemoreflex function were recorded through whole-body plethysmography (EMKA Technologies, France) in freely moving mice. Over the course of 3 h, RB was recorded while mice breathed room air in the plethysmograph [11,12,38,40]. All the experiments were performed between 10:00 and 16:00 h. Animals were habituated to a whole-body plethysmography chamber for two consecutive days prior to recording. On the day of the experiment, a minimum of 2 h was allowed for the mice to acclimatize to the recording chamber. Plethysmograph was flushed at 0.75 L/min [40]. Chamber temperature (23.5 ± 0.1 °C), atmospheric pressure and relative humidity (42.0 ± 2.0 %) were monitored and stable during recordings. Ventilatory parameters as tidal volume (V_T), respiratory frequency (R_f), minute ventilation (V_E: V_T x R_f), inspiratory time (T_i), expiratory time (T_e), total respiratory time (T_{TOT}), peak expiratory flow (PeF), peak inspiratory flow (PiF) were determined using ecgAUTO software (EMKA Technologies, France) [11,12,38,40].

Regularity of resting breathing pattern was quantified by changes in

the breath-to-breath (B–B) interval through SD1 (short axis) and SD2 (long axis) values using 3 segments of ~300 consecutive breaths at rest [11,12,38,40]. Same recordings were used to estimate V_T oscillations and irregularity score (IS) [11,12,38,40]. Breathing disorders (apneas and hypopneas) were quantified in the last hour of resting breathing recordings [11,12,38,40]. Apnea were defined as breathing cessation for at least 3 consecutive respiratory cycles. Hypopneas were defined as reductions in V_T amplitude of <50 % of the normal V_T, for at least 3 respiratory cycles. Sighs were defined as a breath cycle with amplitude >50 % of the average cycle amplitude.

Central chemoreflex function was evaluated following 2 min of hypercapnia (7 % F_iCO_2/93 % F_iO_2). The hypercapnic ventilatory response (HCVR) was obtained by calculating the slope of the V_E between F_iCO_2 0.03 % and 7 % [11,12,38,40].

5.3. RTN oxidative stress

Endogenous superoxide levels in the RTN were measured with fluorescent-dye dihydroethidium (DHE) (Molecular Probes, Life Technologies). Snap-frozen brains were sectioned on a cryostat at 25-μm thickness and placed onto electrostatic-charged microscope slides (Superfrost, VWR Scientific, West Chester, PA). Brain sections containing the ventral surface of medulla (6.6 to bregma for mice) were incubated with 1 μM DHE in PBS for 30 min at 37 °C. Sections were then rinsed three times in PBS for 5 min and mounted with fluorescent mounting medium (Vector Shield, Vector Laboratories). Images were acquired with a confocal Zeiss LSM 710 system (Zeiss, Germany). Images were taken under the same conditions for magnification, intensity, brightness, and gain. Images were analyzed using ImageJ software (NIH, Bethesda, MD).

5.4. Immunofluorescence and Sholl analysis

Mice were deeply anaesthetized with overdose of sodium pentobarbital (100 mg/kg i.p.) and perfused through the ascending aorta with saline solution (NaCl 0.9 %) followed by 4 % phosphate-buffered (0.1 M; pH 7.4) paraformaldehyde (Merck, Germany). The brain was removed and stored in the perfusion fixative for overnight at room temperature and later maintained in 30 % sucrose prior to cryopreservation. All histochemical procedures were performed using free-floating sections (25 μm). Sections were briefly washed in sterile PBS 1X, mounted on charged slides, and dried overnight. For fluorescence immunohistochemistry, sections were rinsed, then incubated with a solution of 1 % Bovine Serum Albumin, 2 % Gelatin and 0.5 % Triton-X in PBS 1x, and then rinsed and incubated with primary antibody at 4 °C overnight. Slices were incubated with a SOD2 mouse mAb (1:500, Santa Cruz), GFAP rabbit mAb GFAP (1:1000, Dako) or Phox2b rabbit mAb (1:500 dilution, Abcam). Sections were then rinsed and incubated with proper secondary antibodies (goat anti-rabbit Alexa 488, Invitrogen; goat anti-mouse Rhodamine-Red, Jackson ImmunoResearch Laboratories) for 60 min at room temperature and rinsed again before mounting on slides. Slides were covered with Vectashield mounting medium (Vectorlabs). To determine the colocalization between SOD2 staining with GFAP or Phox2b, consecutive confocal images were taken using a Zeiss LSM 710 microscope and a 40× oil immersion objective (1.4 NA) at 1 μm intervals. Images were acquired sequentially with three lasers (in nm: 405, 488, 561 and 633), and Z projections were reconstructed using ImageJ (NIH).

For Sholl analysis, fixed brainstem slices containing the RTN with a thickness of 25 μm were obtained and subjected to immunofluorescence staining using primary anti-GFAP rabbit antibody (1:1000, Sigma) with a secondary 488-conjugated antibody from Invitrogen. Z-stacks images were acquired at 0.5 μm using a confocal microscope at 40x. Sholl analysis was performed on astrocytes with non-truncated processes as the main structure. Sholl radius was set at 4 μm from the center of the astrocyte to determine the number of intersections with concentric spheres at increasing radii. The number of intersections was then plotted as a function of distance from the soma, allowing quantification of the complexity and distribution of astrocytic processes. All analysis was performed blinded to the experimental groups to avoid bias using the Simple Neurite Tracer (SNT) plugin for Fiji.

5.5. RTN SOD2 expression

After sacrificing the animals, mice brains were removed and stored at −80 °C. Then, micro-punches containing the RTN were lysed with RIPA buffer +1 % protease inhibitor (Sigma-Aldrich) and sonicated at minimum power for 15 s at 4 °C (Omni Instruments). Protein samples were centrifuged at 14,000 rpm at 4 °C twice for 15 min. Protein concentration was determined using the BCA Protein Assay Kit (Pierce Biotechnology, Rockford, IL). For electrophoresis, 50 μg of total protein was loaded and separated in SDS-PAGE 10 % polyacrylamide gels during 90 min at 90 V. Then, proteins were transferred into PVDF membrane during 2 h and 30 min at 120 mA. SOD2 expression level was assessed by immunoblot using a rabbit polyclonal SOD2 (1:1000, Millipore) in blocking buffer (TBS/Tween-20 0,2 %/Milk 3 %) incubated overnight at 4 °C. Then, membranes were incubated 1 h at room temperature with a horseradish peroxidase-conjugated secondary antibody (anti-rabbit, KPL). Membranes were developed using the Pico West ECL solution (Thermo Scientific) in a dark room. SOD2 expression levels was calculated as the ratio of intensity of the SOD2 band relative to the intensity of the housekeeping protein GAPDH mouse monoclonal antibody (1:1000, Sigma). The analysis of the optical densities of the specific bands was performed with ImageJ software (NIH, USA).

5.6. Analysis of single-cell RNAseq data

Single-cell RNA-sequencing (RNAseq) data from the mouse ventral parafacial brainstem zone were obtained from a publicly available database (GEO number: GSE153172). Cell dissociation, single-cell RNAseq and quality control methods are described in detail in the original report of the database [8]. Data processing and visualization was performed using the Scanpy package 78 (v.1.9.2) in Python (v. 3.8.10). The combined ventral parafacial cells RNAseq dataset was obtained from 3,345 cells with expression data for 5,321 genes. The aggregated counts matrix was normalized by dividing the total count per cell, then multiplied by the median count across all cells. It was then subjected to a base-2 logarithmic transformation and scaled to have zero mean and unit variance column-wise. The computation of principal components (PCs) was carried out using the top 2,000 genes that exhibit the highest variability. Before computing the PCs, genes associated with cell cycle, stress response, the Y-chromosome, hemoglobin, ribosomal, mitochondrial, and the gene Xist were excluded from the list of highly variable genes. To create a batch-balanced nearest-neighbor graph with $k = 10$, the first 20 PCs were utilized. Subsequently, a 2D UMAP embedding was generated. The Leiden community detection algorithm was applied to the k-NN graph at 4 resolutions to assign the initial clusters, resulting in 52 initial clusters. To examine specific Sod2 positive cells, we initially distinguished between Sod2 positive or negative cells by the categorical function. Then, we determine the first 30 PCs and the variance ratio of this PCs. 2D UMAP embedding was generated using Leiden community detection algorithm to define clusters of cells that express Sod2 gene.

5.7. Mitochondrial isolation

Mitochondria were isolated from a mouse brain using a method referenced [28]. Briefly, after dissecting the mouse brain, it was broken down in an MSH-BSA solution (containing mannitol 225 mM, sucrose 75 mM, HEPES 5 mM, EGTA 1 mM, and BSA 0.2 mg/mL, supplemented with a protease inhibitor cocktail). This homogenate was first centrifuged at 600 g for 5 min. The supernatant from this was then centrifuged

again at 8,000×*g* for a duration of 10 min. The pellet resulting from this was mixed with a 12 % Percoll solution in MSH (without BSA) and carefully layered over a 24 % Percoll solution. This setup underwent a final centrifugation at 18,000×*g* for 15 min. Post this, the pellet was cleaned twice and lastly resuspended in MSH. To assess the protein concentration, a BCA Protein Assay Kit by Pierce was employed.

5.8. Measurement of ATP concentration

The ATP generated by isolated mitochondria was evaluated within the supernatant of the isolated mitochondrial fractions. ATP levels were determined using a luciferin/luciferase bioluminescence assay kit (ATP determination kit no. A22066, Molecular Probes, Invitrogen). Subsequently, the ATP content in each sample was calculated based on standard curves and then normalized to the total protein concentration.

5.9. Indirect mitochondrial membrane potential measurement

The mitochondrial membrane potential was assessed using the TMRE method, as previously described [28]. In brief, a mixture of 20 μg of mitochondrial protein in a 100 μL experimental buffer (containing KCl 125 mM, HEPES 20 mM, $MgCl_2$ 2 mM, KH_2PO_4 2.5 mM, BSA 0.1 %, glutamate 5 mM, and malate 5 mM) was left to incubate at 37 °C for 10 min to energize the mitochondria. After this, 100 μL of 2 μM TMRE was introduced, leading to a total volume of 200 μL and bringing the TMRE concentration down to 1 μM. This mixture was incubated once more at 37 °C for 10 min. Post incubation, it was centrifuged at 14,000×*g* for 5 min. To gauge the supernatant, 100 μL was taken and measured. The excess supernatant was removed, with the pellet being reconstituted in another 100 μL of the buffer for analysis. The fluorescence of TMRE was then measured using a fluorometer at 514/570 nm wavelengths for excitation and emission, respectively.

5.10. Statistical analysis

Data is presented as mean ± standard error mean (S.E.M.). Comparisons were performed through T-Student test. The level of significance was defined as $p < 0.05$. Statistical analysis was performed with GraphPad Prism 8.0 software (La Jolla, USA), Seaborn Python open-source library module from Jupyter Notebook version 6.0.3 software and Imaris View 10.1.1 version.

Author contributions

E.D.J. collected, analyzed, and interpreted data, and contributed to the preparation of the manuscript. S.V., H·S.D., C.T., M.A.O, K.S., K.V.P. and R.Q. performed data collection, analysis and contributed to the preparation of the manuscript. R.D.R. performed all *in-vivo* experiments and contributed to the concept of the project, experimental design, data interpretation and preparation of the manuscript. All data collection was undertaken in the laboratory of R.D.R. All authors approved the final version of the manuscript.

Funding

We acknowledge Fondo de Desarrollo Científico y Tecnológico Fondecyt 1220950.

Declaration of competing interest

The authors declare that they have no known competing financial interests or personal relationships that could have appeared to influence the work reported in this paper.

Acknowledgments

We thank Mr. Fidel Flores for his help in managing the animal facility and Mr. Sergio Hernandez for RNAseq script generation.

Appendix A. Supplementary data

Supplementary data to this article can be found online at https://doi.org/10.1016/j.redox.2023.102992.

References

[1] D.C. Andrade, A. Arce-Alvarez, C. Toledo, H.S. Díaz, C. Lucero, H.D. Schultz, N. J. Marcus, R. Del Rio, Exercise training improves cardiac autonomic control, cardiac function, and arrhythmogenesis in rats with preserved-ejection fraction heart failure, J. Appl. Physiol. 123 (3) (1985) 567–577, 2017.

[2] M.P. Baier, R.Y. Nagaraja, H.P. Yarbrough, D.B. Owen, A.M. Masingale, R. Ranjit, M.A. Stiles, A. Murphy, M.P. Agbaga, M. Ahmad, D.M. Sherry, M.T. Kinter, H. Van Remmen, S. Logan, Selective ablation of Sod2 in astrocytes induces sex-specific effects on cognitive function, d-serine availability, and astrogliosis, J. Neurosci. : Offi. J.Soci. Neurosci. 42 (31) (2022) 5992–6006, https://doi.org/10.1523/JNEUROSCI.2543-21.2022.

[3] T.D. Bradley, The ups and downs of periodic breathing: implications for mortality in heart failure, J. Am. Coll. Cardiol. 41 (12) (2003) 2182–2184.

[4] C. Carvalho, P.I. Moreira, Oxidative stress: a major player in cerebrovascular alterations associated to neurodegenerative events, Front. Physiol. 9 (2018) 806, https://doi.org/10.3389/fphys.2018.00806.

[5] C. Carvalho, P.S. Katz, S. Dutta, P.V. Katakam, P.I. Moreira, D.W. Busija, Increased susceptibility to amyloid-beta toxicity in rat brain microvascular endothelial cells under hyperglycemic conditions, J. Alzheimers Dis. 38 (2014) 75–83, https://doi.org/10.3233/JAD-130464.

[6] A.J. Case, J. Tian, M.C. Zimmerman, Increased mitochondrial superoxide in the brain, but not periphery, sensitizes mice to angiotensin II-mediated hypertension, Redox Biol. 11 (2017) 82–90, https://doi.org/10.1016/j.redox.2016.11.011.

[7] Y. Chen, M.B. Azad, S.B. Gibson, Superoxide is the major reactive oxygen species regulating autophagy, Cell Death Differ. 16 (7) (2009) 1040–1052, https://doi.org/10.1038/cdd.2009.49.

[8] C.M. Cleary, B.M. Milla, F.S. Kuo, S. James, W.F. Flynn, P. Robson, D.K. Mulkey, Somatostatin-expressing parafacial neurons are CO2/H+ sensitive and regulate baseline breathing, Elife 10 (2021), e60317, https://doi.org/10.7554/eLife.60317.

[9] C.M. Cleary, T.S. Moreira, A.C. Takakura, M.T. Nelson, T.A. Longden, D.K. Mulkey, Vascular control of the CO2/H+-dependent drive to breathe, Elife 9 (2020), e59499, https://doi.org/10.7554/eLife.59499.

[10] F. Duprat, C. Girard, G. Jarretou, M. Lazdunski, Pancreatic two P domain K+ channels TALK-1 and TALK-2 are activated by nitric oxide and reactive oxygen species, J. Physiol. 562 (Pt 1) (2005) 235–244, https://doi.org/10.1113/jphysiol.2004.071266.

[11] H.S. Díaz, D.C. Andrade, C. Toledo, K.V. Pereyra, K.G. Schwarz, E. Díaz-Jara, C. Lucero, A. Arce-Álvarez, H.D. Schultz, J.N. Silva, A.C. Takakura, T.S. Moreira, N. J. Marcus, R. Del Rio, Episodic stimulation of central chemoreceptor neurons elicits disordered breathing and autonomic dysfunction in volume overload heart failure, Am. J. Physiol. Lung Cell Mol. Physiol. 318 (1) (2020) L27–L40.

[12] E. Díaz-Jara, H.S. Díaz, A. Rios-Gallardo, D. Ortolani, D.C. Andrade, C. Toledo, K. V. Pereyra, K. Schwarz, G. Ramirez, F.C. Ortiz, M.E. Andía, R. Del Rio, Exercise training reduces brainstem oxidative stress and restores normal breathing function in heart failure, Free Radic. Biol. Med. 172 (2021) 470–481, https://doi.org/10.1016/j.freeradbiomed.2021.06.032.

[13] J.M. Flynn, S. Melov, SOD2 in mitochondrial dysfunction and neurodegeneration, Free Radic. Biol. Med. 62 (2013) 4–12, https://doi.org/10.1016/j.freeradbiomed.2013.05.027.

[14] J.M. Flynn, S.W. Choi, N.U. Day, A.A. Gerencser, A. Hubbard, S. Melov, Impaired spare respiratory capacity in cortical synaptosomes from Sod2 null mice, Free Radic. Biol. Med. 50 (7) (2011) 866–873, https://doi.org/10.1016/j.freeradbiomed.2010.12.030.

[15] H.V. Forster, P. Haouzi, J.A. Dempsey, Control of breathing during exercise, Compr. Physiol. 2 (1) (2012) 743–777, https://doi.org/10.1002/cphy.c100045.

[16] R.E. Fulton, J.N. Pearson-Smith, C.Q. Huynh, T. Fabisiak, L.P. Liang, S. Aivazidis, B.A. High, G. Buscaglia, T. Corrigan, R. Valdez, T. Shimizu, M.N. Patel, Neuron-specific mitochondrial oxidative stress results in epilepsy, glucose dysregulation and a striking astrocyte response, Neurobiol. Dis. 158 (2021), 105470, https://doi.org/10.1016/j.nbd.2021.105470.

[17] L. Gao, P. Ortega-Sáenz, A. Moreno-Domínguez, J. López-Barneo, Mitochondrial redox signaling in O2-sensing chemoreceptor cells, Antioxidants Redox Signal. 37 (4–6) (2022) 274–289, https://doi.org/10.1089/ars.2021.0255.

[18] H. Girouard, L. Park, J. Anrather, P. Zhou, C. Iadecola, Angiotensin II attenuates endothelium-dependent responses in the cerebral microcirculation through nox-2-derived radicals, Arterioscler. Thromb. Vasc. Biol. 26 (2006) 826–832, https://doi.org/10.1161/01.ATV.0000205849.22807.6e.

[19] A. Gourine, V. Kasymov, N. Marina, F. Tang, M. Figueiredo, S. Lane, A. Teschemacher, K. Spyer, K. Deisseroth, S. Kasparov, Astrocytes control breathing through pH-dependent release of ATP, Science 329 (2010) 571–575.

[20] P.G. Guyenet, Regulation of breathing and autonomic outflows by chemoreceptors, Compr. Physiol. 4 (4) (2014) 1511–1562, https://doi.org/10.1002/cphy.c140004.
[21] P.G. Guyenet, D.A. Bayliss, Neural control of breathing and CO2 homeostasis, Neuron 87 (5) (2015) 946–961.
[22] P.G. Guyenet, D.A. Bayliss, R.L. Stornetta, M.G. Ludwig, N.N. Kumar, Y. Shi, P. G. Burke, R. Kanbar, T.M. Basting, B.B. Holloway, I.C. Wenker, Proton detection and breathing regulation by the retrotrapezoid nucleus, J. Physiol. 594 (6) (2016) 1529–1551, https://doi.org/10.1113/JP271480.
[23] J. Haorah, N.A. Floreani, B. Knipe, Y. Persidsky, Stabilization of superoxide dismutase by acetyl-l-carnitine in human brain endothelium during alcohol exposure: novel protective approach, Free Radic. Biol. Med. 51 (8) (2011) 1601–1609, https://doi.org/10.1016/j.freeradbiomed.2011.06.020.
[24] T. Kara, K. Narkiewicz, V.K. Somers, Chemoreflexes–physiology and clinical implications, Acta Physiol. Scand. 177 (3) (2003) 377–384, https://doi.org/10.1046/j.1365-201X.2003.01083.x.
[25] Y.S. Kim, P. Gupta Vallur, R. Phaëton, K. Mythreye, N. Hempel, Insights into the dichotomous regulation of SOD2 in cancer, Antioxidants 6 (4) (2017) 86, https://doi.org/10.3390/antiox6040086.
[26] R.M. Lazarenko, T.A. Milner, S.D. Depuy, R.L. Stornetta, G.H. West, J.A. Kievits, D. A. Bayliss, P.G. Guyenet, Acid sensitivity and ultrastructure of the retrotrapezoid nucleus in Phox2b-EGFP transgenic mice, J. Comp. Neurol. 517 (2009) 69–86.
[27] A.A. Miller, T.M. De Silva, C.P. Judkins, H. Diep, G.R. Drummond, C.G. Sobey, Augmented superoxide production by Nox2-containing NADPH oxidase causes cerebral artery dysfunction during hypercholesterolemia, Stroke 41 (2010) 784–789, https://doi.org/10.1161/STROKEAHA.109.575365.
[28] R.G. Mira, R.A. Quintanilla, W. Cerpa, Mild traumatic brain injury induces mitochondrial calcium overload and triggers the upregulation of NCLX in the Hippocampus, Antioxidants 12 (2) (2023) 403, https://doi.org/10.3390/antiox12020403.
[29] D.K. Mulkey, R.L. Stornetta, M.C. Weston, J.R. Simmons, A. Parker, D.A. Bayliss, P. G. Guyenet, Respiratory control by ventral surface chemoreceptor neurons in rats, Nat. Neurosci. 7 (12) (2004) 1360–1369.
[30] K. Narkiewicz, C.A. Pesek, P.J. van de Borne, M. Kato, V.K. Somers, Enhanced sympathetic and ventilatory responses to central chemoreflex activation in heart failure, Circulation 100 (3) (1999) 262–267.
[31] K. Narkiewicz, M. Kato, C.A. Pesek, V.K. Somers, Human obesity is characterized by a selective potentiation of central chemoreflex sensitivity, Hypertension 33 (5) (1999) 1153–1158, https://doi.org/10.1161/01.hyp.33.5.1153 (Dallas, Tex. : 1979).
[32] E. Nattie, A. Li, Central chemoreceptors: locations and functions, Compr. Physiol. 2 (1) (2012) 221–254, https://doi.org/10.1002/cphy.c100083.
[33] K.S. Park, H. Bang, E.Y. Shin, C.H. Kim, Y. Kim, The inhibition of TREK2 channel by an oxidizing agent, 5,5'-dithio-bis (2-nitrobenzoic acid), via interaction with the C-terminus distal to the 353rd amino acid, KOREAN J. PHYSIOL. PHARMACOL. : official journal of the Korean Physiological Society and the Korean Society of Pharmacology 12 (4) (2008) 211–216, https://doi.org/10.4196/kjpp.2008.12.4.211.
[34] P. Ponikowski, S.D. Anker, T.P. Chua, D. Francis, W. Banasiak, P.A. Poole-Wilson, A.J. Coats, M. Piepoli, Oscillatory breathing patterns during wakefulness in patients with chronic heart failure: clinical implications and role of augmented peripheral chemosensitivity, Circulation 100 (24) (1999) 2418–2424.
[35] F. Sesti, S. Liu, S.Q. Cai, Oxidation of potassium channels by ROS: a general mechanism of aging and neurodegeneration? Trends Cell Biol. 20 (1) (2010) 45–51, https://doi.org/10.1016/j.tcb.2009.09.008.
[36] Y. Shi, R.L. Stornetta, D.S. Stornetta, S. Onengut-Gumuscu, E.A. Farber, S. D. Turner, P.G. Guyenet, D.A. Bayliss, Neuromedin B expression defines the mouse retrotrapezoid nucleus, J. Neurosci. 37 (48) (2017) 11744–11757.
[37] C.R. Sobrinho, C.M. Gonçalves, A.C. Takakura, D.K. Mulkey, T.S. Moreira, Fluorocitrate-mediated depolarization of astrocytes in the retrotrapezoid nucleus stimulates breathing, J. Neurophysiol. 118 (3) (2017) 1690–1697.
[38] C. Toledo, D.C. Andrade, C. Lucero, A. Arce-Alvarez, H.S. Díaz, V. Aliaga, H. D. Schultz, N.J. Marcus, M. Manríquez, M. Faúndez, R. Del Rio, Cardiac diastolic and autonomic dysfunction are aggravated by central chemoreflex activation in heart failure with preserved ejection fraction rats, J. Physiol. 595 (8) (2017) 2479–2495.
[39] C. Toledo, D.C. Andrade, C. Lucero, H.D. Schultz, N. Marcus, M. Retamal, C. Madrid, R. Del Rio, Contribution of peripheral and central chemoreceptors to sympatho-excitation in heart failure, J. Physiol. 595 (1) (2017) 43–51, https://doi.org/10.1113/JP272075.
[40] C. Toledo, E. Díaz-Jara, H.S. Diaz, K.G. Schwarz, K.V. Pereyra, A. Las Heras, A. Rios-Gallardo, D.C. Andrade, T. Moreira, A. Takakura, N.J. Marcus, R. Del Rio, Medullary astrocytes mediate irregular breathing patterns generation in chronic heart failure through purinergic P2X7 receptor signalling, EBioMedicine 80 (2022), 104044, https://doi.org/10.1016/j.ebiom.2022.104044.
[41] F. Triposkiadis, G. Karayannis, G. Giamouzis, J. Skoularigis, G. Louridas, J. Butler, The sympathetic nervous system in heart failure physiology, pathophysiology, and clinical implications, J. Am. Coll. Cardiol. 54 (19) (2009) 1747–1762.
[43] H. Tsutsui, S. Kinugawa, S. Matsushima, Oxidative stress and heart failure, Am. J. Physiol. Heart Circ. Physiol. 301 (6) (2011) H2181–H2190.
[44] H. Van Remmen, C. Salvador, H. Yang, T.T. Huang, C.J. Epstein, A. Richardson, Characterization of the antioxidant status of the heterozygous manganese superoxide dismutase knockout mouse, Arch. Biochem. Biophys. 363 (1999) 91–97.
[42] I.C. Trombetta, C. Maki-Nunes, E. Toschi-Dias, M.J. Alves, M.U. Rondon, F. X. Cepeda, L.F. Drager, A.M. Braga, G. Lorenzi-Filho, C.E. Negrao, Obstructive sleep apnea is associated with increased chemoreflex sensitivity in patients with metabolic syndrome, Sleep 36 (1) (2013) 41–49, https://doi.org/10.5665/sleep.2298.